Danger in the dark: Stability of perovskite solar cells with varied stoichiometry and morphology stressed at various conditions

Roja Singh[a,b], Hang Hu[a,b], Thomas Feeney[b], Alexander Diercks[b], Felix Laufer[b], Yang Li[a,b], The Duong[c], Fabian Schackmar[a,b], Bahram A. Nejand[a,b] and Ulrich W. Paetzold[a,b]**

R. Singh, H. Hu, Y. Li, F. Schackmar, B. A. Nejand and U. W. Paetzold

[a] Institute of Microstructure Technology, Karlsruhe Institute of Technology, Hermann-von-Helmholtz-Platz 1, 76344 Eggenstein-Leopoldshafen, Germany

R. Singh, H. Hu, T. Feeney, A. Diercks, F. Laufer, Y. Li, F. Schackmar, B. A. Nejand and U. W. Paetzold

[b] Light Technology Institute, Karlsruhe Institute of Technology, Engesserstrasse 13, 76131 Karlsruhe, Germany

T. Duong

[c] School of Engineering, The Australian National University, Canberra, ACT 2601, Australia

* E-mail: roja.singh@kit.edu ; ulrich.paetzold@kit.edu

KEYWORDS degradation, long-term stability, stoichiometry, quenching, light, temperature

ABSTRACT Long-term stability of perovskite solar cells (PSCs) remains a bottleneck for commercialization. While studies of PSCs stoichiometry and morphology with regard to performance are prevalent, understanding of these factors influence on long-term stability is lacking. In this work, we evaluate the impact of stoichiometry and morphology on the long-term stability of cesium formamidinium based PSCs. We demonstrate that the lead iodide (PbI_2) to formamidinium iodide (FAI) ratio influences stability under various stress factors (elevated temperature and light). A high molar ratio (PbI_2/FAI >1.1) in the perovskite precursor displays drastic degradation under ISOS-L1 (100 mW/cm^2, 25 °C, maximum power point tracking) conditions. However, post-degradation analysis contradicts these results. Devices with PbI_2/FAI ≤1.1 are stable under light but intermittent current density-voltage characterizations indicate that device performance decreases during storage in the dark. Migration of iodide (I^-) to the electron transport layer (ETL) and iodine vacancies ($V_{I^-}^+$) to the hole transport layer (HTL) forms localized shunts in the absorber layer. Pinhole formation, surrounded by FA^+ rich regions, explains the extent of damage in comparably aged films. In summary, this work emphasizes the importance of reporting stability under different stress conditions, coupled with post degradation and dark recovery analysis of PSCs to better understand the complexities of perovskite instability under real-life conditions such as expected during outdoor operation.

1. Introduction

In the last decade, perovskite solar cells (PSCs) have been able to overcome many challenges: improving efficiency,[1] demonstrating scalability,[2,3] avoiding toxicity,[4–6] among the others. One challenge this technology still needs to overcome is long-term stability.[7,8] Organic metal halide semiconductor thin films have many suitable properties for opto-electronic applications but can be intrinsically and extrinsically unstable. The intrinsic stability of perovskites depends on the ionic

radii and percentage fraction of the cations or halides used for the formation of ABX_3. The right choice of the percentage fraction of these constituent chemicals can give perovskites the desired phase stability.[9] However, phase-stable perovskites can still undergo reversible or irreversible degradation upon exposure to oxygen, moisture,[10–12] light and elevated temperature.[13–15] Simultaneously, charge transport layers, electrodes, and interfaces between the perovskite layer and the charge transport layers can also undergo degradation in presence of the above mentioned stress factors.[16,17] Due to the sensitive nature of the perovskite material and other additional layers implemented in the device, one needs to practice caution in the course of the different fabrication and characterization steps. During fabrication, the stoichiometry of the precursor solution and quenching technique controls the nucleation and crystallization in the wet perovskite film. Hence, stoichiometry and morphology can be key for fabrication of high performing PSCs and are more likely to demonstrate long-term stability.[18] Standard testing protocols study the stability of PSCs under different stress conditions: light, elevated temperature, bias voltage, relative humidity, etc.[19] Testing the stability of PSCs under mutual stress factors instead of just one is important. Determining the origin of these instabilities during and post processing can help in understanding and resolving an issue as complex as perovskite instability.

Material stoichiometry affects the crystallization kinetics during the perovskite processing, which is an important factor influencing the phase stability and long-term stability of PSCs. Stoichiometry is controlled by the molar ratio of the precursor ionic compounds in perovskites: AX and BX_2. Here A and B are monovalent and divalent cations respectively and X is a halide. Extensive theoretical calculations and experimental study on the thermodynamics of the material has contributed to development of phase-stable hybrid and inorganic lead halide perovskites.[9,20] However, in-depth understanding of the effects of stoichiometry variations in the perovskite

processing and overall long-term stability still lags behind. Jacobsson *et. al.* explained that the devices with excess lead iodide (PbI_2) had higher hysteresis and exhibited instability under light exposure, whereas devices using deficient PbI_2 precursor generated excess organic species surrounding the grain boundaries that hindered charge-carrier transportation.[21] Ulzii *et. al.* demonstrated that the photolysis of unreacted PbI_2 crystals under continuous light results in formation of metallic lead (Pb_0) and iodine (I_2) in both $MAPbI_3$ and formamidinium (FA) -based PSCs. The presence of Pb_0 acted as a quencher and decreased the performance of PSCs under illumination.[22] On the contrary, A-cation ionic compound excess in the precursor solution is demonstrated to boost the long-term stability of PSCs. To transform the residual PbI_2 at the buried interface to the FA-based perovskite, Gao *et. al.* incorporated formamidinium iodide (FAI) and cesium bromide (CsBr) in tin oxide (SnO_2). This strategy stabilized the lattice strain of the FA-based perovskite near the buried interface, reduced the interfacial defects and increased the photo-stability of device under illumination.[23] Song *et. al.* reported optimum AX excess (<5% of FAI) can be beneficial for long-term stability while maintaining high performance. Perovskites with Pb-rich surfaces exhibited high power conversion efficiency (PCE) but during maximum power point (MPP) tracking, their performance dropped. Though AX-rich perovskites had low initial PCE, their MPP tracking improved over time and stabilized.[24]

Alongside stoichiometry, drying of the wet perovskite film can also control the nucleation and crystallization, determining the film morphology. The final film quality affects the performance and stability of the PSCs. Addition of anti-solvent reduces the solubility of perovskite solution and produces local super-saturation points from where crystallization of the wet film begins.[25] Anti-solvent-quenching (ASQ) is a very conventional technique and widely used for perovskite fabrication.[26] However, this method is a limitation in the up-scaling process. Furthermore,

presence of wrinkles in anti-solvent-quenched films due to fast quenching can increase the roughness of the film. Vacuum quenching (VQ) is an alternative technique extensively used for quenching of large-area devices and modules. Nejand *et. al.* implemented VQ for drying of planar and smooth large-area perovskite films. All perovskite tandems and mini-modules (aperture area 12.25 cm^2) fabricated showed high performance and stability.[27] The effect of different surface morphology due to the choice of quenching technique on the long-term stability has not yet been studied.

Considering the impact of unreacted precursor, defect site, crystallization and lattice strain on the resultant film quality, it is important to quantify how these parameters affect the final device stability. The stability of a perovskite film or a device also depends on the stress factor. Domanski *et. al.* studied the stability of PSCs under different stress factors: light, temperature, relative humidity, electrical bias etc. They emphasized statistical and standardized reporting can help in making reliable comparison of the stability of PSCs. A set of testing protocols were recommended to facilitate a consensus for ageing of PSCs.[28] Chen *et. al.* reported recombination centers formed due to elevated temperature and excess charge carriers were the reason behind rapid light-induced degradation in $MAPbI_3$ solar cells.[29] Li. *et. al.* also studied the effect of different stress factors (heat, light and stabilized power output) on cesium formamidinium lead iodide ($Cs_{0.1}FA_{0.9}PbI_3$).[30] They concluded that the effect of light and stabilized power output was more severe than the effect of elevated temperature. Khenkin *et. al* have studied bias induced degradation of various types of previously developed solar cell technologies in detail.[31] For some perovskite compositions, the effect of elevated temperature might be more detrimental while for others presence of light-induced degradation or electrical bias might cause more damage. To avoid anomalies, implementing testing protocols under different stress conditions is highly recommended. The

international summit on organic photovoltaic stability (ISOS) protocols is tailored suitably by perovskite and organic solar cells community for accelerated testing of the next-generation solar technology.[19]

Real-life outdoor operation of solar cells also includes night periods. Reversible degradation occurring during the day cycle under light and elevated temperature can be compensated for during the night cycle. The dynamics of PSC recovery in dark was first reported by Khenkin *et. al.*[32] The origin of instability in PSCs such as trap formation, ion migration, etc. can affect their performance and determine their ability to recover in the dark affecting their overall long-term stability.[32,33]

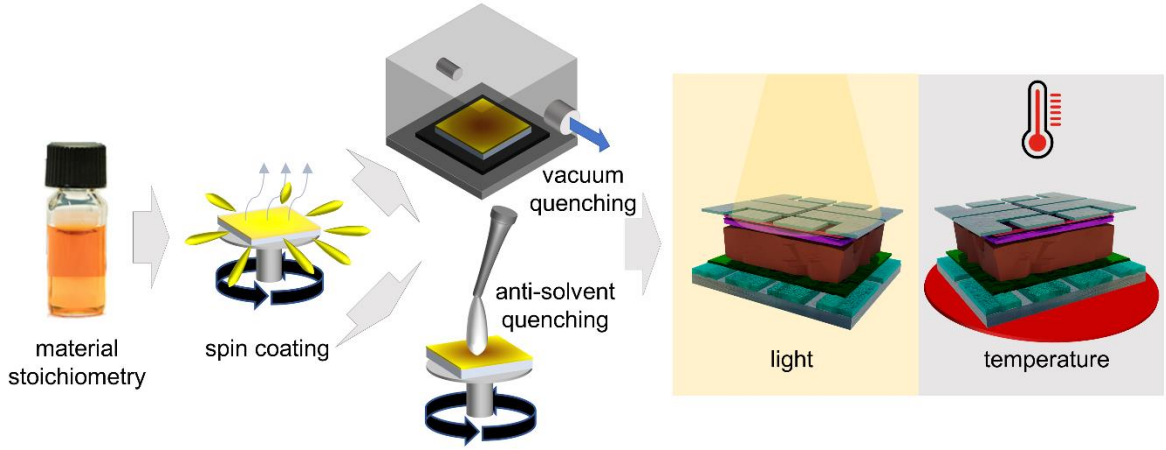

Figure 1: Schematic illustration of the underlying methodology of this study.

In-depth understanding of materials stoichiometry and surface morphology of pure-iodide PSCs to achieve phase stability and high performance has progressed in recent times. However, the effects of varying stoichiometry and diverse morphology on the long-term stability is still not clear. PSCs implementing such variations in stoichiometry and morphology can respond differently to accelerated testing protocols under different stress conditions. Understanding the influence of such variations on degradation mechanism can aid in developing PSCs that are high in performance but also withstand longer durations under standardized tests. In this work, we critically assess

important material properties (stoichiometry and morphology) of $Cs_{0.18}FA_{0.82}PbI_3$ PSCs to elucidate their impact on the long-term stability under different stress conditions i.e. light and elevated temperature as illustrated in **Figure 1**. We evaluate if high performing devices are "universally" stable. We also analyze if devices that are stable under accelerated testing, are also stable in the absence of stress factors, by placing them under dark storage and observing their performance over time.

2. Experimental Section/Methods

2.1. Materials:

Details of the precursors used are as follows. [2-(9H-Carbazol-9-yl)ethyl]phosphonic Acid (2PACz: TCI, CAS: 20999-38-6), Lead iodide (PbI_2: TCI, CAS: 10101-63-0), Formamidinium iodide (FAI: Dyesol, CAS: 879643-71-7), Cesium chloride (CsCl: abcr, CAS: 7647-17-8), Fullerene (C_{60}: 99.5% Sigma Aldrich, CAS: 99685-96-8), Bathocuproine (BCP: Lumtec, CAS: 4733-39-5). Tetrakis (dimethylamino) tin (IV) (99.99%-Sn, TDMASn PURATREM) was purchased from Strem. All solvents namely, N,N-dimethylformamide, ≥99.9% (DMF, CAS: 68-12-2), Dimethyl sulfoxide (DMSO) anhydrous, ≥99.9% CAS: 67- 68-5), ethyl acetate (EA anhydrous, 99.8%, CAS: 141-78-6), 2-Propanol, ≥98%, (IPA, CAS: 67-63-0) were purchased from Sigma-Aldrich. Ethanol absolute 99.8% was purchased from VWR Chemicals.

2.2. PSCs fabrication:

The semi-transparent perovskite solar cells (PSC) with the architecture of glass/ ITO/ 2PACz/ $Cs_{0.18}FA_{0.82}PbI_3$/ C_{60}/ SnO_X / IZO/ Au grid were prepared on 16x16 mm^2-patterned indium doped tin oxide (ITO) substrates with sheet resistance 15 Ω/□ (Luminescence Technology). The substrates were cleaned in an ultra-sonic bath with acetone and isopropyl alcohol followed by oxygen plasma treatment. The concentration of 2PACz solution was 1.8mg /4ml of absolute

Ethanol. 2PACz layer was deposited by spin coating at 3000 rpm followed by annealing at 100 °C for 10 minutes. $Cs_{0.18}FA_{0.82}PbI_3$ perovskite solution was prepared by dissolving 1.1 mmol PbI_2 and 0.18 mmol of CsCl in 1 mL solvent mixture of DMF: DMSO in 4:1 ratio at 130 °C. In a separate glass vial, 1 mmol of FAI was weighed. The cooled solution of PbI_2 and CsCl was added to this vial. The different stoichiometry solutions were prepared by varying molarity of FAI by 0.05M, while molarity of both PbI_2 and CsCl was kept the same. For anti-solvent quenching (ASQ), the perovskite solution was spin coated using a two-step program of 1000-5000 rpm for 10 sec-30 sec. 150 µL of EA was dropped on the center of the substrates at 18 sec of the second step. Vacuum quenching (VQ) was performed in a square vacuum chamber with inlet and outlet at 90 °. The vacuum time of ~30 s was optimized and used for all vacuum-quenched devices. The samples were annealed at 150 °C for 30 minutes in an inert atmosphere. 20nm of C_{60} was thermally evaporated (Angstrom, EvoVac) on top of the perovskite film followed by 30nm of SnO_X deposited by atomic deposition layer (Picosun, r200-advanced). As a top contact, indium doped tin oxide (IZO) was sputtered on top of SnO_X in a (Kurt J. Lesker Company, PVD 75). Finally, gold bands were evaporated (VacTec, COAT 320) on the edges for ease of probing during measurement.

2.3. Measurements and Characterizations:

The current density-voltage (*J-V*) characteristics of the semi-transparent devices were measured using a solar simulator (Newport, Oriel Sol3A) equipped with a source meter (Keithley, 2400) and a xenon lamp. The calibration was achieved using a certified silicon reference solar cell (Fraunhofer) with KG5 filter (Schott). Sample holders (fabricated in-house) with gold pins were used to contact the cells for electrical measurements. The active area of the cell was 0.105 cm^2 and an illumination mask of 0.0784 cm^2 active area was used as an aperture mask during measurement. *J–V* measurements were made at an intensity of 97 mW/cm^2 and were later corrected to 100

mW/cm^2. The temperature of all cells was controlled at 25 °C employing a Peltier element connected to a microcontroller while conducting *J-V* and MPP measurements. External quantum efficiency (EQE) spectra for PSC were measured in a Photovoltaic Device Characterization System (Bentham, PVE300). A monochromatic was used to modulate the xenon lamp. The chopper frequency of 580 Hz with an integration time of 400 ms was used. Transmittance and reflectance of the perovskite films (glass/ ITO/ 2PACz/ $Cs_{0.18}FA_{0.82}PbI_3$) were also measured using an integrating sphere in the same setup. Absorptance was calculated using the formula A = 1 – T – R, where, T is the transmittance and R is reflectance. X-ray diffraction (XRD) was conducted on the perovskite films using a Bruker D2Phaser system with Cu-Kα radiation (λ = 1.5405 Å) in Bragg–Brentano configuration using a LynxEye detector. Scanning electron microscope (SEM) images of the perovskite films were taken using a Zeiss LEO1530 VP scanning electron microscope with an in-lens detector. SEM images were captured using a 5 kV acceleration voltage and an aperture size of 20 µm. Optical microscope (OM) images of the perovskite films were taken using ZEISS Axioplan 2 microscope. Atomic force microscopy (AFM) images of the perovskite films were taken using Nano Wizard II (JPK Instruments). The scanning area was 10 µm × 10 µm. Electro-luminescence (EL) measurement of devices were performed in an in-house built setup with 775 nm short-pass and 760 nm long-pass filters. The modules were biased using a Keithley 2450. Cathodo-luminescence (CL) images of the perovskite films measurements were performed on an FEI Verios SEM equipped with a GatanMonoCL4 Elite. The measurements are performed at 3 kV / 25pA. The images were taken in panchromatic mode with appropriate dichroic filters. Charge extraction (CE), delay-time charge extraction by linearly increasing voltage (Delay-time-CELIV) and Mott Schottky (MS) measurements were measured for devices on PAIOS system by Fluxim AG. Intensity of 69.2 mW/cm^2 with a light-pulse length of 100 µs and a ramp

rate of 40 V/ms was used. Ideality factor was measured for devices on PAIOS system by Fluxim AG. The light intensity from an LED was varied upto 69.2 mW/cm^2 and open circuit voltage decay was measured for the same. MPP tracking were performed under a class A^{++} LED-based solar simulator (Wavelabs, LS-2). The spectrum was a close match to the AM1.5G over the relevant spectral range.

3. Results and discussion

In order to understand the influence of stoichiometry and morphology on long-term stability of $Cs_{0.18}FA_{0.82}PbI_3$ PSCs, we first vary the molar ratio used in our standard process with ASQ. Then, we introduce and compare an alternative solvent-free quenching technique VQ, which is known to produce more planar perovskite films. We study the impact of different surface morphology (grain size, presence or absence of wrinkles, surface roughness, etc.) and crystallization (crystallite size, strain, etc.) on the resulting perovskite films due to the variation of stoichiometry or quenching technique. Finally, by exposing films and complete devices to different accelerated degradation tests, we study the effect of different stress factors (light and elevated temperature) on the previously varied conditions.

The effect of the precursor solution material stoichiometry is pivotal for the device performance and stability.[22,34] In our reference devices $Cs_{0.18}FA_{0.82}PbI_3$, the molarity of PbI_2 and FAI are 1.1 M and 1.0 M respectively. We will refer to the resulting molar ratio (PbI_2/FAI= MR= 1.1) as the standard recipe hereafter. The importance of having excess PbI_2 in the precursor solution for the formation of pinhole-free perovskite layer has been reported previously.[22,35] Cesium chloride (CsCl) is used as a Cs source. The details of device fabrication are explained in the supporting information. Although mixed halide perovskite has a wider appeal, with regard to application to

tandem solar cells, they also have an inherent problem: phase segregation. Hence, to study the effect of the molar ratio PbI_2/FAI, we choose a system $Cs_{0.18}FA_{0.82}PbI_3$ with enhanced stability that did not provide additional complexities such as phase segregation originating from halide components

3.1. Impact of material stoichiometry and quenching technique on the initial performance

In order to study if the performance and stability of the pristine device is affected by variations in stoichiometry, we vary the molarity of FAI in our precursor solution from 0.9 M to 1.1 M in 0.05M increments. FAI variation is chosen as a method to vary stoichiometry as it ensures minimum increment of iodide ions (I^-) in the precursor solution. The molarity of PbI_2 and CsCl in all solutions are kept the same as in the reference devices (as demonstrated in **Table S1**). Five precursor solutions of different MRs: 1.2, 1.15, 1.1, 1.05 and 1.0 (for simplicity rounded to the nearest 0.05) are spin-coated and quenched by the ASQ technique. The annealed films are completed into semi-transparent devices with the following architecture: glass/ ITO/ 2PACz/ $Cs_{0.18}FA_{0.82}PbI_3$/C_{60}/SnO_X/ IZO/ Au grid. Here, ITO is indium doped tin oxide, 2PACz is (2-(9H-carbazol-9-yl) ethyl) phosphonic acid, C_{60} is fullerene, SnO_X is tin oxide, IZO is indium doped zinc oxide and Au is gold. Changing MR in the precursor solution results in slight variation of PCE in the devices as shown in **Figure 2 a**. Devices with MR >1.1 exhibit higher V_{OC} as excess PbI_2 remaining in the precursor solution accumulates to the grain boundaries of the film and provides a passivating effect.[21,35] This reduces non-radiative recombination and increases V_{OC} (**Figure S1 a**). Fill factor (FF) and short circuit current density (J_{SC}) of the devices remain unchanged upon changing MRs (**Figure S1 b** and **Figure S1 c**). J_{SC} values are further verified by EQE measurements (**Figure S2 a**) and support the values shown in **Figure S1 c**. The absorbance of the perovskite films, as presented in **Figure S2 b**, ensures that changing MR does not change

the thickness and hence the amount of light absorbed by the film. First derivative at the inflection point of EQE of the devices provide valuable information about the bandgap of the perovskite material (**Figure S3 a**). It is evident that changing MR of the precursor solution, changes the perovskite material bandgap. For MR of 1.0, 1.1 and 1.2 the measured bandgaps are 1.58, 1.58 and 1.59 eV respectively. This indicated a red shift with respect to increasing MR. This trend in bandgap is also verified by Tauc plot analysis from absorbance measurements (**Figure S3 b**). When the spin-coated films are annealed, the by-product formamidinium chloride (FACl) volatilizes. In a precursor solution with MR> 1.1 (more FAI), more formamidinium ion (FA^+) is incorporated into the crystal lattice for the same amount of cesium ion (Cs^+). This results in a blue shift of the bandgap in the resulting perovskite film.[36] Semi-transparent PSCs are stable when tracked under MPP tracking at 100 mW/cm^2 and 25 °C for up to 300 s as shown in **Figure S4**. In summary, while increasing MR slightly increases average and maximum PCE, minor changes of molar ratio from the optimum does not drastically change the device performance. Devices with higher MR >1.1 exhibit higher V_{OC} because of grain boundary passivation due to excess PbI_2. However, short-term stability (MPP tracking under illumination) is comparable for devices with different stoichiometries.

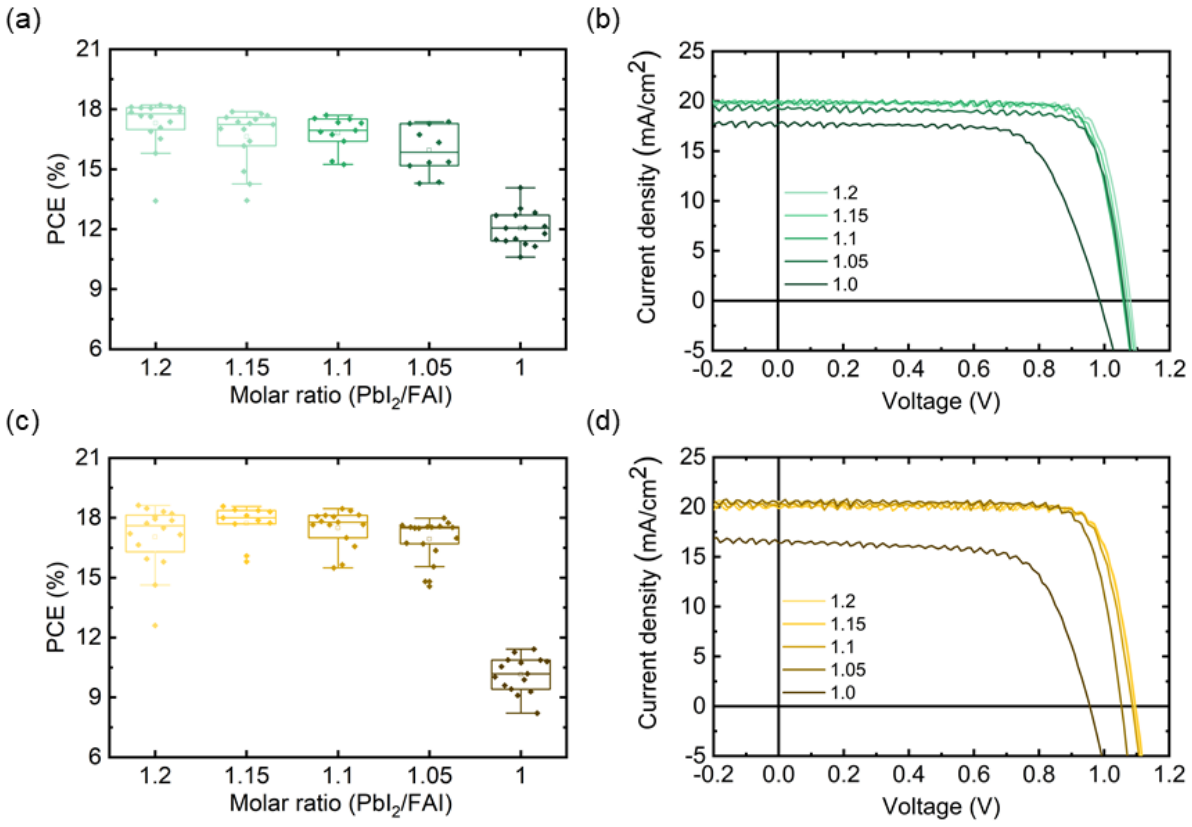

Figure 2: (a) Statistical distribution of power conversion efficiency (PCE) and (b) *J-V* characteristics of the PSCs using an anti-solvent quenching process. (c) Statistical distribution of PCE and (d) *J-V* characteristics of the PSCs using a vacuum quenching process.

Having investigated the effect of stoichiometry, we examine in a second step the influence of quenching technique on device performance and short-term stability by comparing devices fabricated using ASQ and VQ. We fabricate vacuum-quenched devices for the same MRs as ASQ devices, which were fabricated concurrently. In ASQ orthogonal solvents such as chlorobenzene, ethyl acetate, γ-butyl acetone, etc., are dropped dynamically on the precursor solution covered spinning substrates.[25] In VQ, instead of using orthogonal solvent, the spin-coated wet perovskite films are placed in a vacuum chamber and quenched using a vacuum pump.[27] **Figure 2 c** shows that the PCE of vacuum-quenched devices follows the same trend in performance as anti-solvent-

quenched devices for a specific MR. Champion device of each stoichiometry variation along with different quenching techniques are shown in **Table S2**. The *J-V* characterizations of the same are presented in **Figure 2 b** and **Figure 2 d**. The trend in V_{OC} and FF for vacuum-quenched devices are identical with anti-solvent-quenched devices. However, the trend in J_{SC} is slightly different (**Figure S1 d, e** and **f**). Profilometry measurements in **Table S3** show that vacuum-quenched films are thinner than corresponding anti-solvent-quenched films of equivalent MR. While in ASQ film thickness remain constant with respect to MR, the thickness of vacuum-quenched films increases with decreasing MR. In anti-solvent-quenched films additional washing with anti-solvent washes off the excess precursor on the surface.[37] In VQ, excess material stays on the film surface. Upon annealing, the presence of more FA^+ in the precursor solution (with decreasing MR) contributes to formation of thicker films resulting in higher J_{SC}.[38] We also confirm the J_{SC} values of vacuum-quenched devices with EQE (**Figure S2 c**) and they comply with J_{SC} values from *J-V* characterization. The performance of vacuum-quenched devices is on par with anti-solvent-quenched devices with MR 1.0 performing much worse than other MRs for both quenching techniques does. An increase in molarity of FAI results in reduced current transport as discussed previously.[21] In the following discussions, we will focus on only three MRs: 1.2, 1.1 and 1.05 as they allow the largest range in MR possible without a substantial loss of PCE. In summary, we confirm that devices quenched differently still have similar performance with comparable short-term stability (MPP tracking under illumination). If the two quenching techniques result in similarly performing and stable devices, in which aspects are the techniques different?

3.2. Impact of material stoichiometry and quenching technique on morphology and crystallization of perovskite films

To investigate the distinction between the different quenching techniques, we delve further into the details of surface morphology of perovskite films quenched using ASQ and VQ. SEM images of annealed anti-solvent-quenched films presented in **Figure 3 a, b,** and **c** reveals that for MR 1.2, bright PbI_2 grains are visible along with dark perovskite grains.[39] As the molarity of FAI in the precursor solution increases, the perovskite grain size grows and the presence of PbI_2 grains decrease. For MR 1.05 the bright PbI_2 grains completely disappear. CL images provided in **Figure S5** further supports this observation. Hence, PbI_2 assists in crystallization and formation of pinhole-free films and FAI contributes to growth of larger perovskite grains. A similar trend in the formation of perovskite and PbI_2 grains is also observed in vacuum-quenched films as seen in **Figure 3 d, e** and **f**. Surface roughness measurements using AFM verify that surface roughness does not change with stoichiometry (**Figure S6**). OM images in the supporting information (**Figure S7 a, b** and **c**) show the presence of wrinkles in films quenched by ASQ. ASQ technique is a fast process, where orthogonal solvent is dynamically dropped onto the spinning substrate. The intermediate phase during film formation produces an in-plane compressive stress. Meanwhile, the rigid substrate prevents the film from expanding horizontally due to an order of magnitude difference in thermal expansion coefficients for the transparent conductive oxides or glass substrate[40] compared to the perovskite. The resulting stress is released vertically forming hills and valleys, i.e., wrinkles.[41] Wrinkles are not observed in optical microscopy images of vacuum-quenched films (**Figure S7 d, e** and **f**), resulting in wrinkle formation being a distinguishing feature between anti-solvent-quenched and vacuum-quenched films. The hills and the valleys in the wrinkle formation have different carrier lifetime, which could affect the long-term stability of anti-solvent-quenched devices.[42] In summary, changing MR affects the grain size

and residual PbI_2 on the film surface while different quenching technique results in presence or absence of wrinkles on the perovskite film.

To understand if changing MR and quenching technique also affects the crystallization of perovskite films we perform XRD. The XRD pattern of ASQ films of MR 1.2, 1.1 and 1.05 are shown in **Figure 3 g**. The peak at a 2θ of 12.7° corresponds to the PbI_2 (100) peak. MR 1.2 exhibits the highest intensity at 12.7°, confirming the presence of unreacted PbI_2. This ratio also has the lowest intensity for the perovskite PSK (100) plane of α-$FAPbI_3$ at 14.2°. The intensity of PbI_2 (100) peak decreases as the MR decreases while the FAI content in the precursor solution and the intensity of PSK (100) plane increases. This change explains that more FAI is available for reaction with PbI_2 and CsCl to form $Cs_{0.18}FA_{0.82}PbI_3$. With decrease in MR, we also observe PSK (100) plane shift towards lower 2θ. This shift is caused due to the change in *d*-spacing. As more of the large FA^+ cation is incorporated into the crystal structure, compressive strain is released resulting in peak shift to lower 2θ.[43] Along with the shift in 2θ peak, the full width at half maximum (FWHM) of the PSK (100) plane also gets broader with decreasing MR, suggesting larger crystallite size.[44] Formation of secondary phases like δ-$FAPbI_3$ at 11.6° is not observed in this work. **Figure 3 i** confirms that vacuum-quenched films also show a similar trade-off between PbI_2 (100) and PSK (100) peaks. The trend in shifting of the PSK (100) peak to low 2θ and the broadening of FWHM with decreasing MR is observed. In summary, changing MR affects the crystallization of perovskite films. A decrease in MR (more FAI) results in larger crystallite size and release of compressive strain in the crystal lattice. Nevertheless, in differently quenched samples of the same MR, the process of crystallization remains the same.

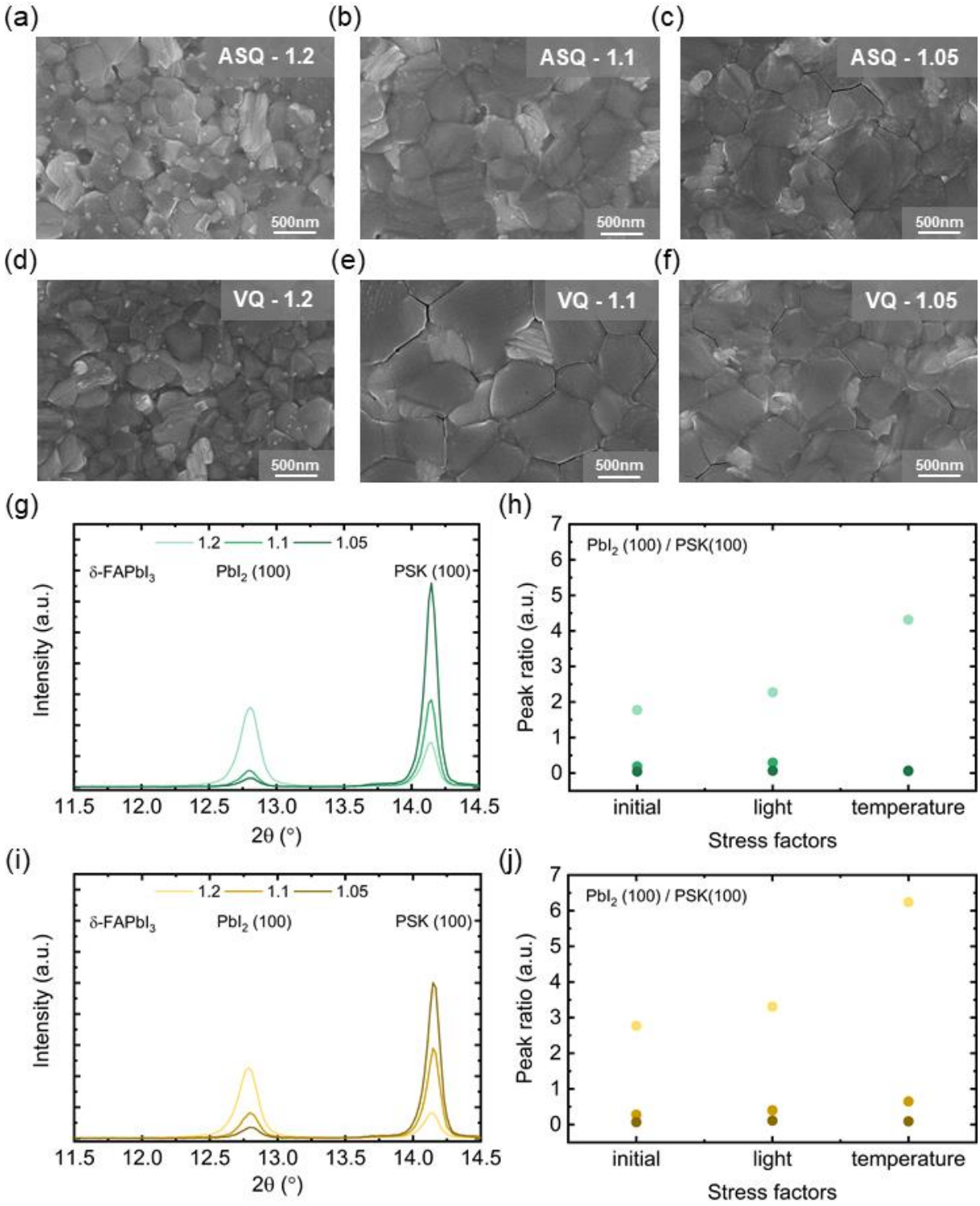

Figure 3: Scanning electron microscope (SEM) images of perovskite thin films with molar ratio (a) 1.2 (b) 1.1 (c) 1.05 quenched using anti-solvent quenching (ASQ) and molar ratio (d) 1.2 (e) 1.1 (f) 1.05 quenched using vacuum quenching (VQ). X-ray diffraction (XRD) pattern of (g) molar

ratio 1.2, 1.1 and 1.05 quenched using ASQ. (h) Peak ratio of lead iodide PbI_2 (100)/ perovskite PSK (100) with molar ratio 1.2, 1.1 and 1.05 quenched using ASQ. XRD pattern of (i) molar ratio 1.2, 1.1 and 1.05 quenched using VQ. (j) Peak ratio of PbI_2 (100)/PSK (100) with molar ratio 1.2, 1.1 and 1.05 quenched using VQ.

Having studied the influence of MR and quenching technique on surface morphology and crystallization, we now investigate how different stress factors like light and elevated temperature affect these differently quenched perovskite layers. In two separate experiments, annealed perovskite films (glass/ ITO/ 2PACz/ $Cs_{0.18}FA_{0.82}PbI_3$) are exposed to light (100 mW/cm^2 and 25 °C) and elevated temperature (dark, 85 °C) for a period of 500 h. XRD is measured on the films before and after the testing period of 500 hours. In a real life scenario, the two mutual stress factors will affect PSCs simultaneously. However, we study their effects separately to understand the different degradation mechanisms triggered by different stress factors. **Figure 3 h** shows the peak ratio of PbI_2 (100) and PSK (100). Increment in the PbI_2 (100)/ PSK (100) peak ratio is inferred as degradation of perovskite layer; with PbI_2 being one of the by-products.[45] Under both testing conditions, there is formation of PbI_2 on aged films. Notably, while full devices with MR 1.2 and MR 1.1 achieved slightly higher PCE than MR 1.05, their corresponding half-stacks exhibit substantially more degradation, counter to initial expectations of higher PCE correlating to increased stability.[18] For both tested stress factors, PbI_2 (100)/ PSK (100) peak ratio was correlated to increasing MR. However, whether the increase in this ratio is correlated to decreased device performance stability is not yet demonstrated. Under light, the increment in ratio of PbI_2 (100)/ PSK (100) is subtle. Elevated temperature testing shows a prominent increment in the peak intensity ratio of PbI_2 (100)/ PSK (100) for MR 1.2. MR$\leq$ 1.1 shows only slight increments in peak intensity ratio under elevated temperature condition. **Figure 3 j** confirms that the PbI_2 (100)/ PSK

(100) peak ratio for vacuum-quenched films also shows similar trend, both in increment intensity and in correlation between degradation and MR. This confirms that, although differently quenched films appear to have different surface morphologies, the same stress condition affects their crystallinity in a similar manner. It should be noted that studying films might not give us complete knowledge about the degradation mechanism that unfolds when complete devices are aged under standard testing protocols. Among the different standardized tests, two tests are chosen for understanding the role of light (ISOS-L1: 100 mW/cm^2, 25 °C, MPP tracking) and elevated temperature (ISOS-D2: dark, 85 °C, intermittent *J-V*) on PSCs.

3.3. Stability of PSCs under ISOS-L1

To compare if the previously observed effects of light on perovskite films also exist with full devices, we expose anti-solvent-quenched semi-transparent devices (glass/ ITO/ 2PACz/ $Cs_{0.18}FA_{0.82}PbI_3$/ C_{60}/ SnO_X / IZO/ Au grid) to the ISOS-L1 test condition. Details of the experimental setup are explained in the supporting information. **Figure 4 a** shows normalized power density at MPP (P_m) in devices with different MRs. MR 1.2 devices initially exhibit some light soaking effect in the first 50 h, however their PCE is overall unstable. This instability is attributed to current density at MPP (J_m), which decreases over the entire 500 h of testing duration (**Figure 4 b**). We attribute the reason for the decreasing J_m to ionic accumulation.[22,46,47] Ionic migration is more pronounced for MR 1.2 because they have a smaller grain-size and more grain boundaries. Grain size affects the activation energy of ionic migration as the activation energy for this process requires a higher energy at the grain interior compared to grain boundaries.[48] The P_m plot of MR 1.1 and 1.05 confirms that ionic migration is severely reduced in devices with a larger grain size, and hence these devices exhibit no ionic accumulation. Therefore, their measurement for the entire duration of 500 h under identical conditions shows stable performance. While a

precursor solution with MR 1.2 (20% excess PbI_2 because of less FAI) boosts performance of the devices due to grain boundary passivation, it also reduces the stability of the devices during MPP tracking under illumination (~10% loss in J_m in 500 h). Voltage at MPP (V_m) for different stoichiometries does not change during the testing period (**Figure S8**). *J-V* characterization and EQE of devices with different stoichiometries before and after ISOS-L1 is compared in **Figure S9**. Hence, we verify that MR 1.2 in the precursor solution is detrimental to the stability of PSCs. However, MR 1.1 (10% excess PbI_2) is an acceptable range resulting in a stable performance as seen in our reference devices. Degradation of vacuum-quenched devices of different stoichiometries are similar to the trend reported above and are presented in **Figure S10** in supporting information.

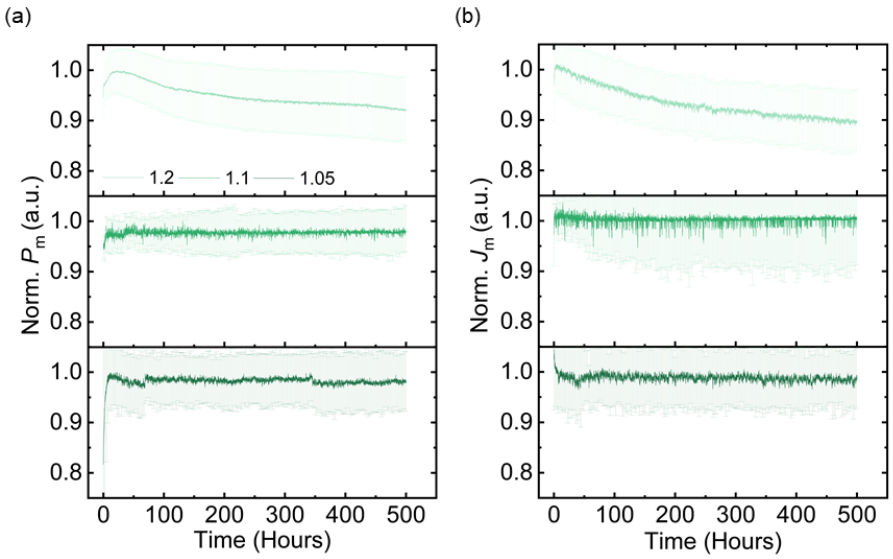

Figure 4: Normalized (a) power, (b) current density at maximum power point (MPP) tracking of anti-solvent-quenched devices of different stoichiometries under ISOS-L1 test condition (100 mW/cm^2, 25 °C, MPP tracking) for 500 hours.

3.4. Stability of PSCs under ISOS-D2

To understand if the effect of having MR >1.1 (less FAI) in the precursor solution is as detrimental on stability under elevated temperature as under illumination; we aged semi-transparent devices of the previously mentioned architecture under the ISOS-D2 condition. Normalized PCE from intermittent *J-V* for MR 1.2, 1.1 and 1.05 are shown in **Figure 5 a**. It is notable that while devices with MR >1.1 and MR <1.1 show a drop in performance, reference devices with MR =1.1 are stable over a period of 500 h. From **Figure 5 b** and **Figure 5 d**, we observe that a drop in V_{OC} and FF is the main reason for decreasing PCE (~10% loss for MR 1.2 and ~5% loss for MR 1.05). Under elevated temperature over a period of 500 h, non-radiative recombination either in the perovskite layer or at interfaces of perovskite layer with charge transport layers, result in a decrease in these parameters.[49,50] Ideality factors calculated for full devices as shown in **Figure S11** support this finding, for MR = 1.1 devices there is no change in the ideality factor before and after ISOS-D2 testing. Comparison of *J-V* characterization and EQE of devices with different stoichiometries before and after ISOS-D2 testing is present in **Figure S12**. Elevated temperature affects vacuum-quenched devices of different stoichiometries in a similar manner and results are presented in **Figure S13**.

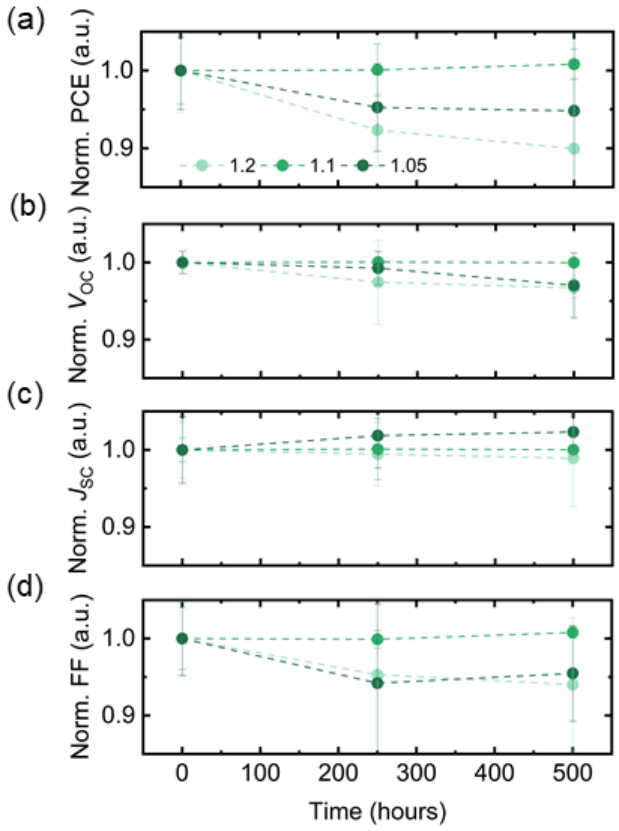

Figure 5: Normalized (a) PCE (b) V_{OC} (c) J_{SC} and (d) FF from *J-V* measurements of ASQ devices of different stoichiometries under ISOS-D2 testing (dark, 85 °C, intermittent *J-V*) for 500 hours.

Having developed understanding about the individual effect of light and elevated temperature stress on the stability of PSCs, it is important to understand the role of mutual stress (simultaneous light and elevated temperature stress) affects the performance of PSCs as such conditions are more realistic to real-life outdoor operation. To understand the same, we performed MPP tracking of anti-solvent-quenched reference (MR 1.1) semi-transparent devices at 100 mW/cm^2 and 85 °C as shown in **Figure S14 a**. As a combined effect of both light and elevated temperature, from **Figure S14 b** we see drop in both J_m and V_m for the champion device. The drop in the former is attributed to ionic accumulation as discussed in ISOS-L1 and the latter is an effect of elevated temperature on the absorber, the charge transport layer or the interfaces as reflected in drop in V_{OC} and FF in

ISOS-D2. Both stress factors contribute to more pronounced ionic accumulation and loss in performance during MPP tracking.

In summary, the degradation mechanisms under different stress conditions are dissimilar, affecting different photovoltaic parameters. Reference devices are stable under both light (ISOS-L1) and elevated temperature (ISOS-D2). Under ISOS-L1 testing, MR >1.1 (less FAI) suffer from ionic accumulation and show a drop in J_m. Under ISOS-D2 for non-standard devices (MR >1.1 and MR <1.1) either the perovskite layer or interfaces of perovskite layer with charge transport layers degrade affecting V_{OC} and FF.

3.5. Analysis of recovery after stress of PSCs

To understand the influence of different stress factors on the recovery dynamics of PSCs, degraded devices are stored in dark under N_2 atmosphere. Intermittent *J-V* characterizations of the degraded devices at intervals of 24 h and 250 h are performed. This time scale is chosen considering stress factors can have either a transient effect on PCE (which recovers on removal of stress factors) or a more permanent effect (which does not recover).[51] There are many reports claiming that PSCs can undergo recovery during storage in the dark, where the effects of degradation can be reversed. [33,52,53] They observe that a PCE decline to 80% of the initial value can be primarily attributed to transient degradation, occurring due to reversible ion migration or metastable defect formation. However, such recovery was not observed beyond when the PSC experienced extensive degradation of up to 50% of the initial PCE.[32] Both transient and permanent trends have been observed in the same devices dependent on the stage of degradation.[54] The radar plot in **Figure 6 a** summarizes the average PCE of devices with different stoichiometries tested under ISOS-D2 and ISOS-L1. The performance of devices post accelerated testing under ISOS-D2 (labelled in red) follows the same trend as during the accelerated testing period. The best

performing reference devices (MR 1.1) show negligible drop in PCE during and after 500 h of testing. However, devices with MR >1.1 (less FAI) and MR <1.1 (more FAI) exhibit reduction in PCE after 24 h (in purple) and 250 h (in brown) of dark storage. This reduction in performance is mainly due to the loss in V_{OC} as shown in **Figure 6 b**. FF of the devices also decreases after 24 h, which recovers partially after 250 h (**Figure S15 b**).

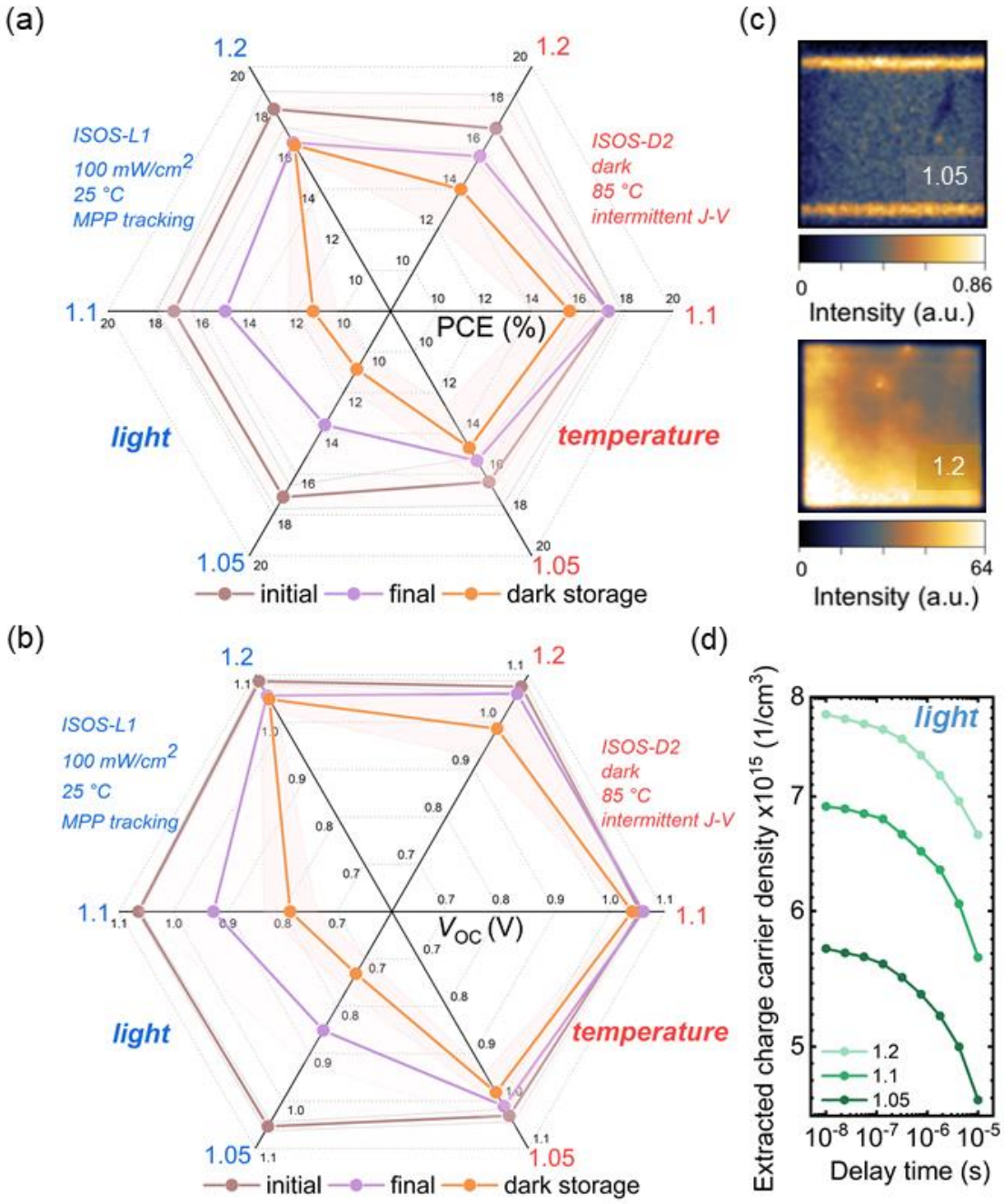

Figure 6: (a) Radar plot of average PCE and (b) radar plot of average V_{OC} of devices with different stoichiometries aged under ISOS-D2 (red) and ISOS-L1 (blue). Devices are measured by *J-V* characterizations before the accelerated testing (brown), after 24 h (purple) and 250 h (orange) of dark storage. (c) Electro-luminescence (EL) images of devices with MR 1.2 and MR 1.05 after dark storage of 250 h post ISOS-L1 testing (d) Extracted charge carrier density of devices with different stoichiometries aged under ISOS-L1 and dark storage of 250 h measured by charge extraction by linearly increasing voltage (CELIV).

During ISOS-L1 testing, we observe that the J_m of devices with MR 1.2 (less FAI) exhibits continuous reduction. However, EQE performed after 24 h of dark storage in **Figure S9** does not show a corresponding reduction in J_{SC}. Redistribution of ionic accumulation during dark storage could possibly cause such behavior.[55] Moreover, the sub-linear dependence of the short-circuit current density on light intensity has been reported previously. The expected decrease in integrated J_{SC} from EQE corresponding to the decrease in J_m from MPP tracking can be observed with increasing incident light intensity during EQE measurement.[56] **Figure S15 b** also confirms this hypothesis, as the FF for MR 1.2 exhibits partial recovery after 250 h of dark storage. Recovery of bias-induced degradation is characterized by improvement of the degraded FF with dark storage.[51] The ability of PSCs to recover in the dark depends on the reason behind the drop in performance. The decrease in performance observed under ISOS-L1 for MR 1.2 can be considered transient degradation due to ionic accumulation at the interface, which are known to be recoverable due to redistribution during dark storage.[57] Simultaneously, deep traps are formed in the perovskite layer under illumination. However, while under persistent illumination, their effect can be masked with photo-generated charge carrier passivation. In dark, with de-trapping of the photo-generated charge carriers, their effect becomes more evident. We report that for FAI-rich stoichiometry,

molar ratio (MR) ≤1.1 the increased deep traps result in drastic decrease in open circuit voltage (V_{OC}) along with drop in short-circuit current density (J_{SC}) and fill factor (FF) when stored in the dark. The drop in the latter two parameters could originate from shallow traps at the interface. The damage done by such deep traps in the perovskite bulk at later stage of degradation are non-recoverable.[32] Performance of devices with MR ≤1.1 (reference devices and devices with more FAI) is severely impacted under dark storage. This reduction in performance can be attributed mainly to formation of deep traps and corresponding loss in V_{OC}.[32] It is noticeable that no recovery of FF of devices with MR ≤1.1 is observed.[51] In summary, all MRs exhibited reduction in performance during storage in dark conditions.

To shed light on the non-recoverable degradation of MR ≤1.1 (reference devices and devices with more FAI) during dark storage, EL was measured on degraded samples. EL images presented for MR 1.2 and MR 1.05 in **Figure 6 c** clearly show that even though devices with MR 1.2 (less FAI) suffer transient degradation under accelerated testing, after dark storage they still show some luminescence related to the local voltage. However, MR 1.05 devices that performed well under ISOS-L1 testing show severe defect distribution during storage in dark and no luminescence.[58] The EL images also exhibits other features.The lines on the top-bottom are gold busbars evaporated to facilitate charge collection from the IZO semi-transparent top contact. The light from the bottom are reflected from the gold busbars and hence they seem more brighter. The variation of luminescence from corner to center is due to the thickness variation of perovskite. Since the EL image provided in **Figure 6 c** is for ASQ, the force of the anti-solvent drop at the center could cause such gradient in the thickness and hence, the variation in the luminescence.

In **Table S1**, we present the reason behind this peculiar behavior of devices tested under ISOS-L1. The existence of localized shunts in devices with different MRs correlates to the amount of

iodide present in the precursor solution. Devices implementing MR ≤1.1 (reference devices and devices with more FAI) have a higher concentration of I^- ions. I^- ions have been reported to exhibit a lower activation energy of 0.1eV as compared to organic cation MA^+ (0.5eV) or Pb^{2+} (0.8eV) ions.[59] According to literature, the I^- ion migration can be activated at room temperature under illumination in presence of bias voltage.[60] It was previously shown that degradation due to I^- ion migration is more prominent in "encapsulated" devices where I_2 species are unable to escape, similar to our semi-transparent devices.[61] As discussed in prior reports in our devices too, I^- ions move towards the electron transport layer (ETL) and iodide vacancies ($V_{I^-}^+$) migrate towards the HTL.[59] In case of higher concentration of iodide ions like in MR 1.05, excessive ion migration can worsen the quality of perovskite. The resulting localized shunts formation visible in optical microscope images of perovskite films on HTLs aged under identical conditions (100 mW/cm^2 light at 25°C) as presented in **Figure S16**. Pinhole formation surrounded by light hued FA^+ rich region in films gives a clearer picture of the damage that occurs inside a complete device, especially at the HTL side. The migration of $I^-/V_{I^-}^+$ and their accumulation at the ETL/HTL respectively promotes non-radiative recombination in the PSCs as observed in our devices with loss in V_{OC} and FF. Further inspection of the loss in V_{OC} with MS analysis (depicted in **Figure S17**) reveals that the built-in potential (V_{bi}) of the MR 1.2 devices show the most impressive recovery to 1.00 V during dark storage after V_{bi} drops drastically to 0.89 V post ISOS-L1 testing. In comparison, while MR 1.1 and MR 1.05 exhibited an initial higher V_{bi}, they do not show any recovery in V_{bi} post dark storage. This trend in recovery of V_{bi} are further backed by the EL results. Formation of localized shunts could cause a drop in V_{bi} resulting in increase in minority charge carrier recombination and reduction in V_{OC} as observed in **Figure 6 b**.[62,63] CELIV measurements in **Figure 6 d** also supports this hypothesis. With delayed extraction time, recombination in MR

1.1 and 1.05 results in fewer charge carriers being extracted as compared to MR 1.2. **Figure S18** confirms that such decay in the charge carrier extraction is not observed for devices degraded under ISOS-D2. Recent literature provides many options to cater the problem of iodine migration reported in this article. Increased large and small cation incorporation or inclusion of Cl^-, can help mitigate the challenge of iodide ion migration.[64–67] Recovery of PSCs under mutual stress factors is beyond the scope of this study.

Hence, we encourage the community to observe the impact of such a phenomenon occurring under dark conditions more carefully by performing post degradation and dark recovery analysis. The consequences are highly relevant for outdoor measurements as the effects are most likely to propagate to the next diurnal cycle.[52,68] Proper reporting of post degradation and dark recovery analysis aids in understanding the impact of material stoichiometry of PSCs and tackling the repercussion of such ambiguous phenomenon.

4. Conclusion

This work reports the influence of material properties (stoichiometry and morphology) on the long-term stability of PSCs under different stress conditions (light and elevated temperature). Our investigations reveal that in spite of the stability in presence of light, I^- ion migration and $V_{I^-}^+$ creation can affect the device performance in the dark. The impact of I^- ion migration and $V_{I^-}^+$ creation can go unnoticed while performing outdoor operation due to the existence of mutual stress factors. However, its effect can propagate to the next diurnal cycle and have severe consequences on long-term stability.

By comparing quenching techniques that result in the presence of wrinkles (ASQ) or in their absence (VQ), we demonstrate that the long-term stability of the equivalent composition perovskites is independent of film morphology. Comparing different stoichiometries, we show

that, for similar perovskite stoichiometries, the highest initial PCE (MR = 1.2) does not correlate to long-term device stability under light or elevated temperature exposure. These results runs contrary to established theory,[18] and indicate that ancillary effects are responsible for previously reported correlations between performance and stability.

Furthermore, we illustrate the need for more robust stability testing by demonstrating that devices which are initially stable under light exposure show formation of localized shunts during storage in dark. We isolate the mechanism for this degradation as being due to I^- ions migrating towards the ETL under illumination (in presence of bias). Resultant $V_{I^-}^+$ defects move towards the HTL inducing non-radiative recombination.in the perovskite absorber The presence of I^- species, which is a boon for harvesting photons in the infrared range, making PSCs viable in the PV industry, is actually a bane on the long run, and the reason behind their permanent degradation. Hence, proper reporting of stability under different stress factors (light and elevated temperature) is imperative. Emphasis on post degradation as well as dark recovery analysis can contribute to understanding and mitigating the influence of such undesirable phenomena occurring in the dark.

ASSOCIATED CONTENT

Supporting Information. The supplementary information is available free of charge.at
It contains additional information about the change in statistical distribution of photovoltaic parameters (V_{OC}, J_{SC}, FF), EQE, bandgap variation and absorptance w.r.t change in molar ratio. Comparision of *J-V*, EQE and bandgap variation before and after accelarated testing (ISOS-L1 and ISOS-D2) are also included. Results of characterizations like CL, AFM, OM, MS and CELIV are also made available (file type, i.e., PDF)

AUTHOR INFORMATION

Corresponding Author

Roja Singh - Institute of Microstructure Technology, Karlsruhe Institute of Technology, Hermann-von-Helmholtz-Platz 1, 76344 Eggenstein-Leopoldshafen, Germany; Light Technology Institute, Karlsruhe Institute of Technology, Engesserstrasse 13, 76131 Karlsruhe, Germany; Email: roja.singh@kit.edu

Ulrich W. Paetzold - Institute of Microstructure Technology, Karlsruhe Institute of Technology, Hermann-von-Helmholtz-Platz 1, 76344 Eggenstein-Leopoldshafen, Germany; Light Technology Institute, Karlsruhe Institute of Technology, Engesserstrasse 13, 76131 Karlsruhe, Germany; Email: ulrich.paetzold@kit.edu

Authors

Roja Singh - Institute of Microstructure Technology, Karlsruhe Institute of Technology, Hermann-von-Helmholtz-Platz 1, 76344 Eggenstein-Leopoldshafen, Germany; Light Technology Institute, Karlsruhe Institute of Technology, Engesserstrasse 13, 76131 Karlsruhe, Germany

Hang Hu - Institute of Microstructure Technology, Karlsruhe Institute of Technology, Hermann-von-Helmholtz-Platz 1, 76344 Eggenstein-Leopoldshafen, Germany; Light Technology Institute, Karlsruhe Institute of Technology, Engesserstrasse 13, 76131 Karlsruhe, Germany

Thomas Feeney - Light Technology Institute, Karlsruhe Institute of Technology, Engesserstrasse 13, 76131 Karlsruhe, Germany;

Alexander Diercks - Light Technology Institute, Karlsruhe Institute of Technology, Engesserstrasse 13, 76131 Karlsruhe, Germany;

Felix Laufer - Light Technology Institute, Karlsruhe Institute of Technology, Engesserstrasse 13, 76131 Karlsruhe, Germany;

Yang Li - Institute of Microstructure Technology, Karlsruhe Institute of Technology, Hermann-von-Helmholtz-Platz 1, 76344 Eggenstein-Leopoldshafen, Germany; Light Technology Institute, Karlsruhe Institute of Technology, Engesserstrasse 13, 76131 Karlsruhe, Germany;

The Duong - School of Engineering, The Australian National University, Canberra, ACT 2601, Australia;

Fabian Schackmar - Institute of Microstructure Technology, Karlsruhe Institute of Technology, Hermann-von-Helmholtz-Platz 1, 76344 Eggenstein-Leopoldshafen, Germany; Light

Technology Institute, Karlsruhe Institute of Technology, Engesserstrasse 13, 76131 Karlsruhe, Germany;
Bahram A. Nejand - Institute of Microstructure Technology, Karlsruhe Institute of Technology, Hermann-von-Helmholtz-Platz 1, 76344 Eggenstein-Leopoldshafen, Germany; Light Technology Institute, Karlsruhe Institute of Technology, Engesserstrasse 13, 76131 Karlsruhe, Germany;

Author Contributions

R.S., F.S., U.W.P. and B.A. conceptualized the project, R.S. performed device fabrication and investigations, H.H. and T.F. assisted with device fabrication, A.D. performed SEM characterization, F.L. performed EL characterization, Y.L. performed AFM characterization, T.D. performed CL characterization. U.W.P. supervised the project. The manuscript was written through contributions of all authors. All authors have given approval to the final version of the manuscript.

Funding Sources

Financial support by the Initiating and Networking funding of the Helmholtz Association (Project Zeitenwende and the Solar Technology Acceleration Platform (Solar TAP)), the program-oriented funding IV of the Helmholtz Association (Materials and Technologies for the Energy Transition, Topic 1: Photovoltaics and Wind Energy, Code: 38.01.04), the German Federal Ministry for Economic Affairs and Climate Action (BMWK) through the projects 27Plus6 (03EE1056B) and SHAPE (03EE1123A), and the Karlsruhe School of Optics and Photonics (KSOP) is gratefully acknowledged.

ACKNOWLEDGMENT

The authors thank the whole “perovskite taskforce” at KIT for fruitful discussions and assistance.

REFERENCES

(1) NREL *Best Research-Cell Efficiency Chart* https://www.nrel.gov/pv/cell-efficiency.html (accessed Dec 3, 2023).

(2) Yan, J.; Savenije, T. J.; Mazzarella, L.; Isabella, O. Progress and Challenges on Scaling up of Perovskite Solar Cell Technology. *Sustain. Energy Fuels* **2022**, *6* (2), 243–266.

(3) Kim, D. H.; Whitaker, J. B.; Li, Z.; van Hest, M. F. A. M.; Zhu, K. Outlook and Challenges of Perovskite Solar Cells toward Terawatt-Scale Photovoltaic Module Technology. *Joule* **2018**, *2* (8), 1437–1451.

(4) Schileo, G.; Grancini, G. Lead or No Lead? Availability, Toxicity, Sustainability and Environmental Impact of Lead-Free Perovskite Solar Cells. *J. Mater. Chem. C* **2021**, *9* (1), 67–76.

(5) Su, P.; Liu, Y.; Zhang, J.; Chen, C.; Yang, B.; Zhang, C.; Zhao, X. Pb-Based Perovskite Solar Cells and the Underlying Pollution behind Clean Energy: Dynamic Leaching of Toxic Substances from Discarded Perovskite Solar Cells. *J. Phys. Chem. Lett.* **2020**, *11* (8), 2812–2817.

(6) Liu, W. W.; Wu, T. H.; Liu, M. C.; Niu, W. J.; Chueh, Y. L. Recent Challenges in Perovskite Solar Cells Toward Enhanced Stability, Less Toxicity, and Large-Area Mass Production. *Adv. Mater. Interfaces* **2019**, *6* (9), 1801758.

(7) Correa-Baena, J. P.; Saliba, M.; Buonassisi, T.; Grätzel, M.; Abate, A.; Tress, W.; Hagfeldt, A. Promises and Challenges of Perovskite Solar Cells. *Science.* **2017**, *358* (6364), 739–744.

(8) Wang, D.; Wright, M.; Elumalai, N. K.; Uddin, A. Stability of Perovskite Solar Cells. *Sol. Energy Mater. Sol. Cells* **2016**, *147*, 255–275.

(9) Park, B. wook; Seok, S. Il. Intrinsic Instability of Inorganic–Organic Hybrid Halide Perovskite Materials. *Adv. Mater.* **2019**, *31* (20), 1805337.

(10) Matteocci, F.; Cinà, L.; Lamanna, E.; Cacovich, S.; Divitini, G.; Midgley, P. A.; Ducati, C.; Di Carlo, A. Encapsulation for Long-Term Stability Enhancement of Perovskite Solar Cells.

Nano Energy **2016**, *30*, 162–172.

(11) Emery, Q.; Remec, M.; Paramasivam, G.; Janke, S.; Dagar, J.; Ulbrich, C.; Schlatmann, R.; Stannowski, B.; Unger, E.; Khenkin, M. Encapsulation and Outdoor Testing of Perovskite Solar Cells: Comparing Industrially Relevant Process with a Simplified Lab Procedure. *ACS Appl. Mater. Interfaces* **2022**, *14* (4), 5159–5167.

(12) Cheacharoen, R.; Boyd, C. C.; Burkhard, G. F.; Leijtens, T.; Raiford, J. A.; Bush, K. A.; Bent, S. F.; McGehee, M. D. Encapsulating Perovskite Solar Cells to Withstand Damp Heat and Thermal Cycling. *Sustain. Energy Fuels* **2018**, *2* (11), 2398–2406.

(13) Cheng, Y.; Ding, L. Pushing Commercialization of Perovskite Solar Cells by Improving Their Intrinsic Stability. *Energy Environ. Sci.* **2021**, *14* (6), 3233–3255.

(14) Akbulatov, A. F.; Luchkin, S. Y.; Frolova, L. A.; Dremova, N. N.; Gerasimov, K. L.; Zhidkov, I. S.; Anokhin, D. V.; Kurmaev, E. Z.; Stevenson, K. J.; Troshin, P. A. Probing the Intrinsic Thermal and Photochemical Stability of Hybrid and Inorganic Lead Halide Perovskites. *J. Phys. Chem. Lett.* **2017**, *8* (6), 1211–1218.

(15) Zhao, J.; Deng, Y.; Wei, H.; Zheng, X.; Yu, Z.; Shao, Y.; Shield, J. E.; Huang, J. Strained Hybrid Perovskite Thin Films and Their Impact on the Intrinsic Stability of Perovskite Solar Cells. *Sci. Adv.* **2017**, *3* (11), eaao5616.

(16) Cheacharoen, R.; Rolston, N.; Harwood, D.; Bush, K. A.; Dauskardt, R. H.; McGehee, M. D. Design and Understanding of Encapsulated Perovskite Solar Cells to Withstand Temperature Cycling. *Energy Environ. Sci.* **2018**, *11* (1), 144–150.

(17) Domanski, K.; Correa-Baena, J. P.; Mine, N.; Nazeeruddin, M. K.; Abate, A.; Saliba, M.; Tress, W.; Hagfeldt, A.; Grätzel, M. Not All That Glitters Is Gold: Metal-Migration-Induced Degradation in Perovskite Solar Cells. *ACS Nano* **2016**, *10* (6), 6306–6314.

(18) Titan, N.; Hartono, P.; Köbler, H.; Graniero, P.; Khenkin, M.; Schlatmann, R.; Ulbrich, C.; Abate, A. Supplementary Information Stability Follows Efficiency Based on the Analysis of a Large Perovskite Solar Cells Ageing Dataset. *Nat. Commun.* **2023**, *14*, 4869.

(19) Khenkin, M. V.; Katz, E. A.; Abate, A.; Bardizza, G.; Berry, J. J.; Brabec, C.; Brunetti, F.; Bulović, V.; Burlingame, Q.; Di Carlo, A.; Cheacharoen, R.; Cheng, Y. B.; Colsmann, A.; Cros, S.; Domanski, K.; Dusza, M.; Fell, C. J.; Forrest, S. R.; Galagan, Y.; Di Girolamo, D.; Grätzel, M.; Hagfeldt, A.; von Hauff, E.; Hoppe, H.; Kettle, J.; Köbler, H.; Leite, M. S.; Liu, S. (Frank); Loo, Y. L.; Luther, J. M.; Ma, C. Q.; Madsen, M.; Manceau, M.; Matheron, M.; McGehee, M.; Meitzner, R.; Nazeeruddin, M. K.; Nogueira, A. F.; Odabaşı, Ç.; Osherov, A.; Park, N. G.; Reese, M. O.; De Rossi, F.; Saliba, M.; Schubert, U. S.; Snaith, H. J.; Stranks, S. D.; Tress, W.; Troshin, P. A.; Turkovic, V.; Veenstra, S.; Visoly-Fisher, I.; Walsh, A.; Watson, T.; Xie, H.; Yıldırım, R.; Zakeeruddin, S. M.; Zhu, K.; Lira-Cantu, M. Consensus Statement for Stability Assessment and Reporting for Perovskite Photovoltaics Based on ISOS Procedures. *Nat. Energy* **2020**, *5* (1), 35–49.

(20) Ciccioli, A.; Latini, A. Thermodynamics and the Intrinsic Stability of Lead Halide Perovskites $CH_3NH_3PbX_3$. *J. Phys. Chem. Lett.* **2018**, *9* (13), 3756–3765.

(21) Jacobsson, T. J.; Correa-Baena, J. P.; Halvani Anaraki, E.; Philippe, B.; Stranks, S. D.; Bouduban, M. E. F.; Tress, W.; Schenk, K.; Teuscher, J.; Moser, J. E.; Rensmo, H.; Hagfeldt, A. Unreacted PbI_2 as a Double-Edged Sword for Enhancing the Performance of Perovskite Solar Cells. *J. Am. Chem. Soc.* **2016**, *138* (32), 10331–10343.

(22) Tumen-Ulzii, G.; Qin, C.; Klotz, D.; Leyden, M. R.; Wang, P.; Auffray, M.; Fujihara, T.; Matsushima, T.; Lee, J. W.; Lee, S. J.; Yang, Y.; Adachi, C. Detrimental Effect of Unreacted PbI_2 on the Long-Term Stability of Perovskite Solar Cells. *Adv. Mater.* **2020**, *32* (16),

1905035.

(23) Gao, Y.; Ren, F.; Sun, D.; Li, S.; Zheng, G.; Wang, J.; Raza, H.; Chen, R.; Wang, H.; Liu, S.; Yu, P.; Meng, X.; He, J.; Zhou, J.; Hu, X.; Zhang, Z.; Qiu, L.; Chen, W.; Liu, Z. Elimination of Unstable Residual Lead Iodide near the Buried Interface for the Stability Improvement of Perovskite Solar Cells. *Energy Environ. Sci.* **2023**, *16* (5), 2295–2303.

(24) Song, W.; Zhang, X.; Lammar, S.; Qiu, W.; Kuang, Y.; Ruttens, B.; Haen, J. D. '; Vaesen, I.; Conard, T.; Abdulraheem, Y.; Aernouts, T.; Zhan, Y.; Poortmans, J. Critical Role of Perovskite Film Stoichiometry in Determining Solar Cell Operational Stability: A Study on the Effects of Volatile A-Cation Additives. *Cite This ACS Appl. Mater. Interfaces* **2022**, *14*, 27922−27931.

(25) Ghosh, S.; Mishra, S.; Singh, T. Antisolvents in Perovskite Solar Cells: Importance, Issues, and Alternatives. *Adv. Mater. Interfaces* **2020**, *7* (18), 2000950.

(26) Liang, Z.; Zhang, Y.; Xu, H.; Chen, W.; Liu, B.; Zhang, J.; Zhang, H.; Wang, Z.; Kang, D.-H.; Zeng, J.; Gao, X.; Wang, Q.; Hu, H.; Zhou, H.; Cai, X.; Tian, X.; Reiss, P.; Xu, B.; Kirchartz, T.; Xiao, Z.; Dai, S.; Park, N.-G.; Ye, J.; Pan, X. Homogenizing Out-of-Plane Cation Composition in Perovskite Solar Cells. *Nature* **2023**, *624*, 557–563.

(27) Abdollahi Nejand, B.; Ritzer, D. B.; Hu, H.; Schackmar, F.; Moghadamzadeh, S.; Feeney, T.; Singh, R.; Laufer, F.; Schmager, R.; Azmi, R.; Kaiser, M.; Abzieher, T.; Gharibzadeh, S.; Ahlswede, E.; Lemmer, U.; Richards, B. S.; Paetzold, U. W. Scalable Two-Terminal All-Perovskite Tandem Solar Modules with a 19.1% Efficiency. *Nat. Energy* **2022**, *7* (7), 620–630.

(28) Domanski, K.; Alharbi, E. A.; Hagfeldt, A.; Grätzel, M.; Tress, W. Systematic Investigation of the Impact of Operation Conditions on the Degradation Behaviour of Perovskite Solar

Cells. *Nat. Energy* **2018**, *3* (1), 61–67.

(29) Chen, B.; Song, J.; Dai, X.; Liu, Y.; Rudd, P. N.; Hong, X.; Huang, J.; Chen, B.; Dai, X.; Rudd, P. N.; Huang, J.; Song, J.; Hong, X.; Liu, Y. Synergistic Effect of Elevated Device Temperature and Excess Charge Carriers on the Rapid Light-Induced Degradation of Perovskite Solar Cells. *Adv. Mater.* **2019**, *31* (35), 1902413.

(30) Li, N.; Luo, Y.; Chen, Z.; Niu, X.; Zhang, X.; Lu, J.; Kumar, R.; Jiang, J.; Liu, H.; Guo, X.; Lai, B.; Brocks, G.; Chen, Q.; Tao, S.; Fenning, D. P.; Zhou, H. Microscopic Degradation in Formamidinium-Cesium Lead Iodide Perovskite Solar Cells under Operational Stressors. *Joule* **2020**, *4* (8), 1743–1758.

(31) Khenkin, M. V.; Anoop, K. M.; Katz, E. A.; Visoly-Fisher, I. Bias-Dependent Degradation of Various Solar Cells: Lessons for Stability of Perovskite Photovoltaics. *Energy Environ. Sci.* **2019**, *12* (2), 550–558.

(32) Khenkin, M. V.; Anoop, K. M.; Visoly-Fisher, I.; Kolusheva, S.; Galagan, Y.; Di Giacomo, F.; Vukovic, O.; Patil, B. R.; Sherafatipour, G.; Turkovic, V.; Rubahn, H. G.; Madsen, M.; Mazanik, A. V.; Katz, E. A. Dynamics of Photoinduced Degradation of Perovskite Photovoltaics: From Reversible to Irreversible Processes. *ACS Appl. Energy Mater.* **2018**, *1* (2), 799–806.

(33) Yadav, P.; Prochowicz, D.; Alharbi, E. A.; Zakeeruddin, S. M.; Grätzel, M. Intrinsic and Interfacial Kinetics of Perovskite Solar Cells under Photo and Bias-Induced Degradation and Recovery. *J. Mater. Chem. C* **2017**, *5* (31), 7799–7805.

(34) Boyd, C. C.; Shallcross, R. C.; Moot, T.; Kerner, R.; Bertoluzzi, L.; Onno, A.; Kavadiya, S.; Chosy, C.; Wolf, E. J.; Werner, J.; Raiford, J. A.; de Paula, C.; Palmstrom, A. F.; Yu, Z. J.; Berry, J. J.; Bent, S. F.; Holman, Z. C.; Luther, J. M.; Ratcliff, E. L.; Armstrong, N. R.;

McGehee, M. D. Overcoming Redox Reactions at Perovskite-Nickel Oxide Interfaces to Boost Voltages in Perovskite Solar Cells. *Joule* **2020**, *4* (8), 1759–1775.

(35) Liu, F.; Dong, Q.; Wong, M. K.; Djurišić, A. B.; Ng, A.; Ren, Z.; Shen, Q.; Surya, C.; Chan, W. K.; Wang, J.; Ng, A. M. C.; Liao, C.; Li, H.; Shih, K.; Wei, C.; Su, H.; Dai, J. Is Excess PbI2 Beneficial for Perovskite Solar Cell Performance? *Adv. Energy Mater.* **2016**, *6* (7), 1502206.

(36) McMeekin, D. P.; Sadoughi, G.; Rehman, W.; Eperon, G. E.; Saliba, M.; Hörantner, M. T.; Haghighirad, A.; Sakai, N.; Korte, L.; Rech, B.; Johnston, M. B.; Herz, L. M.; Snaith, H. J. A Mixed-Cation Lead Mixed-Halide Perovskite Absorber for Tandem Solar Cells. *Science (80-.).* **2016**, *351* (6269), 151–155.

(37) Al-Ashouri, A.; Magomedov, A.; Roß, M.; Jošt, M.; Talaikis, M.; Chistiakova, G.; Bertram, T.; Márquez, J. A.; Köhnen, E.; Kasparavičius, E.; Levcenco, S.; Gil-Escrig, L.; Hages, C. J.; Schlatmann, R.; Rech, B.; Malinauskas, T.; Unold, T.; Kaufmann, C. A.; Korte, L.; Niaura, G.; Getautis, V.; Albrecht, S. Conformal Monolayer Contacts with Lossless Interfaces for Perovskite Single Junction and Monolithic Tandem Solar Cells. *Energy Environ. Sci.* **2019**, *12* (11), 3356–3369.

(38) Ji, R.; Zhang, Z.; Cho, C.; An, Q.; Paulus, F.; Kroll, M.; Löffler, M.; Nehm, F.; Rellinghaus, B.; Leo, K.; Vaynzof, Y. Thermally Evaporated Methylammonium-Free Perovskite Solar Cells. *J. Mater. Chem. C* **2020**, *8* (23), 7725–7733.

(39) Gharibzadeh, S.; Fassl, P.; Hossain, I. M.; Rohrbeck, P.; Frericks, M.; Schmidt, M.; Duong, T.; Khan, M. R.; Abzieher, T.; Nejand, B. A.; Schackmar, F.; Almora, O.; Feeney, T.; Singh, R.; Fuchs, D.; Lemmer, U.; Hofmann, J. P.; Weber, S. A. L.; Paetzold, U. W. Two Birds with One Stone: Dual Grain-Boundary and Interface Passivation Enables >22% Efficient

Inverted Methylammonium-Free Perovskite Solar Cells. *Energy Environ. Sci.* **2021**, *14* (11), 5875–5893.

(40) Liu, K.; Wang, Z.; Qu, S.; Ding, L. Stress and Strain in Perovskite/Silicon Tandem Solar Cells. *Nano-Micro Lett.* **2023**, *15* (1), 1–5.

(41) Bush, K. A.; Rolston, N.; Gold-Parker, A.; Manzoor, S.; Hausele, J.; Yu, Z. J.; Raiford, J. A.; Cheacharoen, R.; Holman, Z. C.; Toney, M. F.; Dauskardt, R. H.; McGehee, M. D. Controlling Thin-Film Stress and Wrinkling during Perovskite Film Formation. *ACS Energy Lett.* **2018**, *3* (6), 1225–1232.

(42) Kim, S. G.; Kim, J. H.; Ramming, P.; Zhong, Y.; Schötz, K.; Kwon, S. J.; Huettner, S.; Panzer, F.; Park, N. G. How Antisolvent Miscibility Affects Perovskite Film Wrinkling and Photovoltaic Properties. *Nat. Commun.* **2021**, *12* (1), 1–10.

(43) Moghadamzadeh, S.; Hossain, I. M.; Jakoby, M.; Abdollahi Nejand, B.; Rueda-Delgado, D.; Schwenzer, J. A.; Gharibzadeh, S.; Abzieher, T.; Khan, M. R.; Haghighirad, A. A.; Howard, I. A.; Richards, B. S.; Lemmer, U.; Paetzold, U. W. Spontaneous Enhancement of the Stable Power Conversion Efficiency in Perovskite Solar Cells. *J. Mater. Chem. A* **2020**, *8* (2), 670–682.

(44) Kim, G.; Min, H.; Lee, K. S.; Lee, D. Y.; Yoon, S. M.; Seok, S. Il. Impact of Strain Relaxation on Performance of A-Formamidinium Lead Iodide Perovskite Solar Cells. *Science* **2020**, *370* (6512), 108–112.

(45) Cui, Y.; Chen, C.; Li, C.; Chen, L.; Singh Bista, S.; Liu, X.; Li, Y.; Awni, R. A.; Song, Z.; Yan, Y. Correlating Hysteresis and Stability with Organic Cation Composition in the Two-Step Solution-Processed Perovskite Solar Cells. *Cite This ACS Appl. Mater. Interfaces* **2020**, *12*, 10588–10596.

(46) Roose, B.; Dey, K.; Chiang, Y. H.; Friend, R. H.; Stranks, S. D. Critical Assessment of the Use of Excess Lead Iodide in Lead Halide Perovskite Solar Cells. *J. Phys. Chem. Lett.* **2020**, *11* (16), 6505–6512.

(47) Thiesbrummel, J.; Le Corre, V. M.; Peña-Camargo, F.; Perdigón-Toro, L.; Lang, F.; Yang, F.; Grischek, M.; Gutierrez-Partida, E.; Warby, J.; Farrar, M. D.; Mahesh, S.; Caprioglio, P.; Albrecht, S.; Neher, D.; Snaith, H. J.; Stolterfoht, M. Universal Current Losses in Perovskite Solar Cells Due to Mobile Ions. *Adv. Energy Mater.* **2021**, *11* (34), 2101447.

(48) McGovern, L.; Koschany, I.; Grimaldi, G.; Muscarella, L. A.; Ehrler, B. Grain Size Influences Activation Energy and Migration Pathways in MAPbBr3Perovskite Solar Cells. *J. Phys. Chem. Lett.* **2021**, *12* (9), 2423–2428.

(49) Zheng, X.; Chen, B.; Yang, M.; Wu, C.; Orler, B.; Moore, R. B.; Zhu, K.; Priya, S. The Controlling Mechanism for Potential Loss in $CH_3NH_3PbBr_3$ Hybrid Solar Cells. *ACS Energy Lett.* **2016**, *1* (2), 424–430.

(50) Shao, S.; Liu, J.; Fang, H. H.; Qiu, L.; ten Brink, G. H.; Hummelen, J. C.; Koster, L. J. A.; Loi, M. A. Efficient Perovskite Solar Cells over a Broad Temperature Window: The Role of the Charge Carrier Extraction. *Adv. Energy Mater.* **2017**, *7* (22), 1701305.

(51) Prete, M.; Khenkin, M. V.; Glowienka, D.; Patil, B. R.; Lissau, J. S.; Dogan, I.; Hansen, J. L.; Leißner, T.; Fiutowski, J.; Rubahn, H. G.; Julsgaard, B.; Balling, P.; Turkovic, V.; Galagan, Y.; Katz, E. A.; Madsen, M. Bias-Dependent Dynamics of Degradation and Recovery in Perovskite Solar Cells. *ACS Appl. Energy Mater.* **2021**, *4* (7), 6562–6573.

(52) Huang, F.; Jiang, L.; Pascoe, A. R.; Yan, Y.; Bach, U.; Spiccia, L.; Cheng, Y. B. Fatigue Behavior of Planar $CH_3NH_3PbI_3$ Perovskite Solar Cells Revealed by Light on/off Diurnal Cycling. *Nano Energy* **2016**, *27*, 509–514.

(53) Vu, T. H. Y.; Chen, W.; Deng, X.; Lau, C. F. J.; Huang, S.; Ho-Baillie, A.; Jia, B.; Wen, X. Visualizing the Impact of Light Soaking on Morphological Domains in an Operational Cesium Lead Halide Perovskite Solar Cell. *J. Phys. Chem. Lett.* **2020**, *11* (1), 136–143.

(54) Khenkin, M. V.; Anoop, K. M.; Visoly-Fisher, I.; Galagan, Y.; Di Giacomo, F.; Patil, B. R.; Sherafatipour, G.; Turkovic, V.; Rubahn, H. G.; Madsen, M.; Merckx, T.; Uytterhoeven, G.; Bastos, J. P. A.; Aernouts, T.; Brunetti, F.; Lira-Cantu, M.; Katz, E. A. Reconsidering Figures of Merit for Performance and Stability of Perovskite Photovoltaics. *Energy Environ. Sci.* **2018**, *11* (4), 739–743.

(55) Caprioglio, P.; Smith, J. A.; Oliver, R. D. J.; Dasgupta, A.; Choudhary, S.; Farrar, M. D.; Ramadan, A. J.; Lin, Y. H.; Christoforo, M. G.; Ball, J. M.; Diekmann, J.; Thiesbrummel, J.; Zaininger, K. A.; Shen, X.; Johnston, M. B.; Neher, D.; Stolterfoht, M.; Snaith, H. J. Open-Circuit and Short-Circuit Loss Management in Wide-Gap Perovskite p-i-n Solar Cells. *Nat. Commun. 2023 141* **2023**, *14* (1), 1–13.

(56) Katz, E. A.; Mescheloff, A.; Visoly-Fisher, I.; Galagan, Y. Light Intensity Dependence of External Quantum Efficiency of Fresh and Degraded Organic Photovoltaics. *Sol. Energy Mater. Sol. Cells* **2016**, *144*, 273–280.

(57) Domanski, K.; Roose, B.; Matsui, T.; Saliba, M.; Turren-Cruz, S.-H. H.; Correa-Baena, J.-P. P.; Carmona, C. R.; Richardson, G.; Foster, J. M.; De Angelis, F.; Ball, J. M.; Petrozza, A.; Mine, N.; Nazeeruddin, M. K.; Tress, W.; Grä, M.; Steiner, U.; Hagfeldt, A.; Abate, A.; Grätzel, M.; Steiner, U.; Hagfeldt, A.; Abate, A.; Grä, M.; Steiner, U.; Hagfeldt, A.; Abate, A. Migration of Cations Induces Reversible Performance Losses over Day/Night Cycling in Perovskite Solar Cells. *Energy Environ. Sci.* **2017**, *10* (2), 604–613.

(58) Soufiani, A. M.; Tayebjee, M. J. Y.; Meyer, S.; Ho-Baillie, A.; Sung Yun, J.; McQueen, R.

W.; Spiccia, L.; Green, M. A.; Hameiri, Z. Electro- and Photoluminescence Imaging as Fast Screening Technique of the Layer Uniformity and Device Degradation in Planar Perovskite Solar Cells. *J. Appl. Phys.* **2016**, *120* (3), 35702.

(59) Azpiroz, J. M.; Mosconi, E.; Bisquert, J.; De Angelis, F. Defect Migration in Methylammonium Lead Iodide and Its Role in Perovskite Solar Cell Operation. *Energy Environ. Sci.* **2015**, *8* (7), 2118–2127.

(60) Lee, J. W.; Kim, S. G.; Yang, J. M.; Yang, Y.; Park, N. G. Verification and Mitigation of Ion Migration in Perovskite Solar Cells. *APL Mater.* **2019**, *7* (4), 041111.

(61) Bitton, S.; Tessler, N. Perovskite Ionics – Elucidating Degradation Mechanisms in Perovskite Solar Cells via Device Modelling and Iodine Chemistry. *Energy Environ. Sci.* **2023**, *16* (6), 2621–2628.

(62) Sundqvist, A.; Sandberg, O. J.; Nyman, M.; Smått, J. H.; Österbacka, R. Origin of the S-Shaped JV Curve and the Light-Soaking Issue in Inverted Organic Solar Cells. *Adv. Energy Mater.* **2016**, *6* (6), 1502265.

(63) Sandberg, O. J.; Kurpiers, J.; Stolterfoht, M.; Neher, D.; Meredith, P.; Shoaee, S.; Armin, A. On the Question of the Need for a Built-In Potential in Perovskite Solar Cells. *Adv. Mater. Interfaces* **2020**, *7* (10), 2000041.

(64) Cai, Q.; Yao, Y.; Lu, Y.; Wang, M.; Zhang, Y.; Song, D.; Xu, Z.; Li, X.; Wei, D. Stable Perovskite Solar Cells with 22% Efficiency Enabled by Inhibiting Migration/Loss of Iodide Ions. *Phys. Chem. Chem. Phys.* **2023**, *25* (9), 6955–6962.

(65) Saidaminov, M. I.; Kim, J.; Jain, A.; Quintero-Bermudez, R.; Tan, H.; Long, G.; Tan, F.; Johnston, A.; Zhao, Y.; Voznyy, O.; Sargent, E. H. Suppression of Atomic Vacancies via Incorporation of Isovalent Small Ions to Increase the Stability of Halide Perovskite Solar

Cells in Ambient Air. *Nat. Energy 2018 38* **2018**, *3* (8), 648–654.

(66) Sun, D.; Gao, Y.; Raza, H.; Liu, S.; Ren, F.; Hu, X.; Wang, H.; Meng, X.; Wang, J.; Chen, R.; Sun, H.; He, J.; Zhou, J.; Pan, Y.; Sun, Z.; Chen, W.; Liu, Z. Chemical Reduction of Iodine Impurities and Defects with Potassium Formate for Efficient and Stable Perovskite Solar Cells. *Adv. Funct. Mater.* **2023**, *33* (41), 2303225.

(67) Wu, W. Q.; Rudd, P. N.; Ni, Z.; Van Brackle, C. H.; Wei, H.; Wang, Q.; Ecker, B. R.; Gao, Y.; Huang, J. Reducing Surface Halide Deficiency for Efficient and Stable Iodide-Based Perovskite Solar Cells. *J. Am. Chem. Soc.* **2020**, *142* (8), 3989–3996.

(68) Jiang, L.; Lu, J.; Raga, S. R.; Sun, J.; Lin, X.; Huang, W.; Huang, F.; Bach, U.; Cheng, Y. B. Fatigue Stability of $CH_3NH_3PbI_3$ Based Perovskite Solar Cells in Day/Night Cycling. *Nano Energy* **2019**, *58*, 687–694.

TOC graphic